COMMUNICATION

Soft Microrobots Employing Nonequilibrium Actuation via Plasmonic Heating

Ahmed Mourran, Hang Zhang, Rostislav Vinokur, and Martin Möller**

Self-propelling micro-objects or colloids are a topical research subject for soft matter microrobots as well as for devices that mix, sort, and circulate fluids.[1] These microswimmers are expected to open new avenues for a biomimetic soft matter microtechnology. Recent literature on synthetic or man-made microswimmers focuses mostly on thermo- and diffusiophoresis for the propulsion. Yet, examples of self-propelling microorganisms in nature teach us also other concepts for propulsion based on complex body deformations. These organisms propel by a shape deformation with distinct spatiotemporal patterns, which consists of a rotational forward movement or a cyclic beating comprising a distinct forward and reverse stroke. The actuation is achieved by rotary motors like in *Escherichia coli*,[2] or by dynein motors that produces bending waves like in sperms and in ciliated protozoa,[3] as well as by whole body deformations as observed for marine phytoplankton *Eutreptiella gymnastica*.[4] Actually within a strict definition, directional swimming may be regarded as a forward motion by shape deformation.[5,6] For the sake of clarity we will use the term "morphing microswimmer" here for locomotion by shape deformation. In contrast to a macroscopic swimmer, such locomotion of small, lightweight microorganisms must take account of the fact that it takes place at very small Reynolds numbers, $R_e \approx 10^{-4}$. In a Newtonian fluid and at $R_e < 1$, inertia and momentum become insignificant when compared to the viscous resistance of the medium. Under these conditions propulsion by a repeated body shape deformation requires nonidentical forward and backward strokes. Precisely, this involves cyclic shape deformation whereby any point on the body traces a loop in space thanks to the different shape configurations in each half-cycle.[7] This famous problem has been pointed out originally by Purcell and is often discussed as the scallop theorem.[5] In order to fulfill the requirement for movement, a body deformation must be composed from different deformation modes, that follow a different time dependence on the forward and the shape recovery stroke, such like bending and torsion or orthogonal bending modes (see also ref. [8] for review). Swimming microbes naturally follow this requirement and it is also mandatory for an artificial microswimmer. Additional requirements for the design of such a morphing microswimmer are a source of energy, sufficiently fast action, and a control mechanism for the repetition as well as for directing the motion.

As a consequence of these multifold requirements, an artificial morphing microswimmer is notoriously difficult to realize. To our knowledge, only three examples have been reported so far. One example is a flexible flagellum-like tail of magnetic particles bridged by DNA molecules and end-linked to a red blood cell as a head. The structure could be actuated and directed by an oscillating external magnetic field.[9] The second example is a biohybrid swimmer that consists of a polydimethylsiloxane filament on which cardiomyocytes have been adhered. The cardiomyocytes contract periodically and deform the filament to propel the swimmer.[10] Only recently, a rather advanced fully synthetic material design was reported in which a liquid crystalline elastomer with photoisomerizable azobenzene groups was propelled by intrabody shape changes as a traveling wave along the object.[11] Irrespective of the fact, that the objects had to be sufficiently large to see the optical pattern, directed motion was fully controlled from outside. Yet, the report can be seen as a major breakthrough because the body shape deformation was caused by a peristaltic motion with the high rates, necessary for the propulsion of such small objects.

In view of this state of knowledge, it remains a challenge to devise new expedient actuation mechanisms for a morphing microswimmer with fast cyclic sequences of shape configurations leading to translational motion. It has been our objective to design an actuation principle that enables further miniaturization and is not bound to the spatial resolution of an external field variation. Furthermore on one side the modes of motion should be programmed by the structure and on the other side can be controlled by the energy uptake. For this purpose we focused on a rotating helix as shown in the scheme of **Figure 1**. Different than in the case of the bacterium *E. coli*, the flagellum cannot simply rotate because we lack a suitable rotary motor. So the forward propulsion must be generated by conformational changes, i.e., body shape variations, which in turn can be exploited for rotation. Necessarily such a body shape deformation must comprise a cyclic process at whose end the object is again in its starting conformation. The first deformation, e.g., unwinding of the helix, must be followed by shape restoring deformations that are not reverse in space in order to cause the required disparity in the viscous forward and backward drag. As pointed out above, this requires conformational changes that are composed from different modes that follow a different time dependence on the forward and the shape recovery stroke. As will be demonstrate below, the combination of different

Dr. A. Mourran, H. Zhang, Dr. R. Vinokur, Prof. M. Möller
DWI-Leibniz Institute for Interactive Materials
RWTH Aachen University
Forckenbeck str. 50, D-52056 Aachen, Germany
E-mail: mourran@dwi.rwth-aachen.de; moeller@dwi.rwth-aachen.de

DOI: 10.1002/adma.201604825

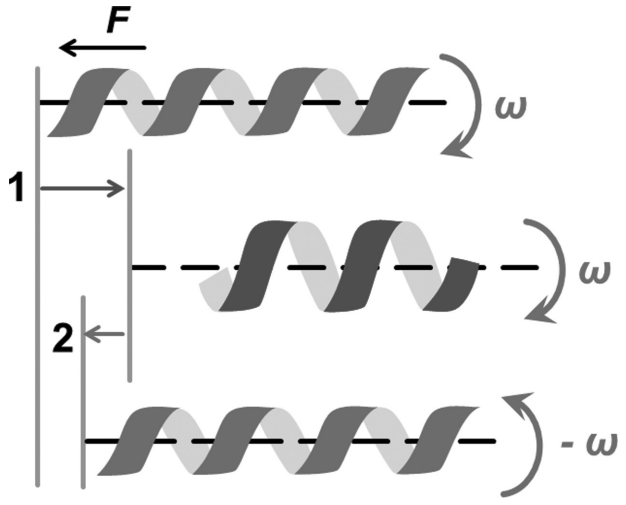

Figure 1. Illustration of the locomotion generated by non-reciprocal deformations of the helix.

deformation modes can be achieved by exploiting the transformation of volume changes to bending modes as it is well known for heterogeneously structured objects.[12,13] In order to achieve the necessary disparity in the forward and the backward mode we operate the system strongly off equilibrium, under conditions where small variations in the input of energy cause strong variations in the response. A key point is to achieve a fast and repetitive response without changing the state of the environment. For this purpose, we exploit the light effectuated thermal response, i.e., swelling/unswelling, of a purposefully designed hydrogel body. We demonstrate that the out-of-equilibrium response can yield precise and fast shape deformations with a rigorous and versatile control of complex motility modes as needed for mobile microscale robots.

Mechanical actuation also in nature is frequently caused by swelling and unswelling of hydrogels. In cases like the hydraulic opening and closing of a pine cone this is not tied to mechanisms of living matter. Still the motion can be fast and complex.[14] Intrigued by these examples, an increasing interest has develped in artificial hydrogel actuator systems that exploit swelling/unswelling in response to an external stimulus.[15] Mostly these systems utilize the volume phase transition of polyacrylamide derivatives and focus on the shape variance between end states in equilibrium.[16] So far, dissipative internal stimulation has been reported by means of an oscillatory chemical reaction[17] and theoretically evaluated for its potential to design morphing microswimmers.[18,19] Yet, most of these systems suffer from a slow stimulus, i.e., change in temperature, pH, or ionic strength, a slow, diffusion-controlled volume response of a hydrogel,[20,21] and the requirement for a cyclic motion that results in a net translation.

Here, we focus on temperature responsive thin poly(*N*-isopropylacrylamide) microgel bodies that undergo bending and torsional motions upon swelling and unswelling. Very fast temperature jumps localized to the volume of the thin microgel body are achieved by photothermal heating of gold nanorods that have been embedded within the poly(*N*-isopropylacrylamide) (PNIPAm) microgel. Irradiation by near IR-light and conversion to heat has been engineered to enable temperature jumps up to more than 20 °C within less than milliseconds (see Supporting Information). Because the heating is restricted to the inner volume of the small microgel objects, they also cool down quickly due to the fast heat transfer to the surrounding bath once the heating is ceased. Because swelling and shrinkage are diffusion controlled and cannot follow in time the fast temperature changes, the volume change can be effectuated out of equilibrium. Under nonequilibrium conditions, the time dependent volume change is controlled by the actual dimensions of the microgel, i.e., the diffusion path, and varies with the dimension of the microgel object. As a consequence volumetric changes of anisometric gels tend to be inhomogeneous. The resulting stress results in shape deformations and the accumulation of elastic energy that is released with a delay. In principle, all these different effects can be well controlled, i.e., temperature change and its rate, dynamic inhomogeneity in swelling, and shrinking, as well as their transformation to bending and torsional modes, and, finally, the built up of elastic stress, that is released in a retarded manner. Below we will demonstrate by the example of a simple hydrogel ribbon in water, how to control the actual motion, i.e., volume change, bending, and torsional motions in their direction, amplitude, and speed. This can be done in such a way, that the ribbon not only adopts a purposeful spatial configuration, but also undergoes cyclic variations in its spatial configuration that follow a different forward and backward path in space and thus creates a thrust to propel the microgel body in water.

Microgels were fabricated by the PRINT technique, known to be effective in controlling the composition, size, and geometry (Figure S2 and S3, Supporting Information).[22] The gelation reaction was carried out in micromolds with a homogeneous dimethyl sulfoxide (DMSO) solution of NIPAm monomer, crosslinker (*N*,*N*′-methylene-bisacrylamide), photoinitiator, and gold nanorods (GNR). The maximum of the longitudinal plasmon absorption was at 791 nm. The later were grafted beforehand with poly(ethylene glycol), PEG. The PEG-brush enables dispersion and trapping of the nanorods within the PNIPAM mesh. The number density of the gold nanorods was adjusted to 9 GNRs per cubic micrometer, which corresponds to a volume fraction of <0.01% and an average rod to rod distance <500 nm. When the gel objects as prepared with DSMO were brought into cold water, a better solvent than DMSO, they swelled by 61% (in 1D, e.g., length). When the water was heated above the collapse temperature they shrunk by 9% relative to the as-prepared state. Based on the degree of swelling in water and the molar ratio of crosslinker to monomer, we estimate the degree of polymerization between crosslinks to about 70 monomer units corresponding to $\langle r \rangle = 5$ nm. This mesh size was confirmed by infiltration experiments with vitamin B12, cytochrome C, and blue dextran yielding colored gels only for the two smaller dyes (see Supporting Information). Suspended gel micro-objects were studied by optical microscopy regarding their reaction to laser light with a spot diameter of about 1 mm. The large spot diameter ensures homogeneous irradiation of the much smaller objects. For experimental details and the image analysis, we refer to the Supporting Information.

In order to evaluate the response of the gels we studied laser actuation of a hydrogel disk with an as-prepared diameter of

30 μm and a thickness of 5 μm. Corresponding to the concentration of 9 GNRs per cubic micrometer, the OD in the normal direction was 0.12. Upon slow heating from outside, the equilibrium diameter changed continuously, corresponding to the volume phase transition of the nonionic hydrogel. Upon irradiation by laser-light at 808 nm and as the power was slowly increased, the diameter showed a sharp transition from the swollen to the collapsed state at an irradiation of power of 1.7 W mm^{-2} (Figure S8ab, Supporting Information). The sharp transition can be expected because the volume concentration of heating elements (GNRs) increased upon the collapse. When the disk was stroboscopically irradiated at high laser power (1.7 W mm^{-2}) and frequencies in the range of 0.5–5 Hz, heating intervals were too short to raise the temperature sufficiently for a full collapse. Because of the fast heat transfer to the outside of the gel body, the intervals between the illumination times allowed efficient cooling (the water temperature was controlled externally at 20 °C, a temperature well below the transition temperature of the PolyNIPAm gel). In order to gain insight into the course of temperature changes during stroboscopic irradiation we mounted a thermistor in a capillary filled with a solution of AuNRs as well as in a corresponding gel layer (Figure S5, Supporting Information). For a solution, the temperature varies sinusoidal with time as depicted in **Figure 2**a as it can be expected because of the ultrafast light to heat conversion in the nanorods (ps) and the fast heat transfer to the surrounding water (ns). In a gel, the temperature tends to increase in an accelerated manner, because of the increase in the density of the nanorods (Figure S4, Supporting Information). Figure 2b depicts the volume change as expressed by the variation in the diameter of the gel disk. For the smallest on-off frequency, the maximum change in diameter of 7 μm at 0.5 Hz corresponded to a $\Delta T \leq 6.2$ °C according to the equilibrium volume phase transition curve (Figure S8, Supporting Information). Volume change starts with high rate and then slows down within the actual actuation cycle. The observation that the volume change and the temperature change are obviously not synchronized, although they occur in phase, gives a first indication that the volume transition change takes place out of equilibrium. The nonequilibrium dynamics becomes even more evident, when one considers the frequency changes of the initial rates of the shrinkage and expansion of the disk diameter. While the rate upon shrinkage does not change (20 μm s^{-1}), the rate upon expansion is largest for long stroboscopic intervals (37 μm s^{-1}).

A strong deviation from the equilibrium transition course might be surprising taking into account that according to the collective diffusion model,[20] the time needed to transport water molecules out of a gel of 5 μm thickness, that shrinks linearly by 10% can be estimated to about 25 ms. Such a short diffusion time should allow near-to-equilibrium repetitive actuation amplitudes for irradiation cycles within the range of 1 s and even less. However, another cause for nonequilibrium dynamics became evident when we imaged the surface of a quickly shrinking hydrogel film by a confocal microscope. Upon irradiation the surface of the film started to wrinkle as shown by the scattering contrast in Figure 2c (inset). Wrinkling indicates the formation of a skin layer as it is expected when the water escapes the surface layers more quickly than from

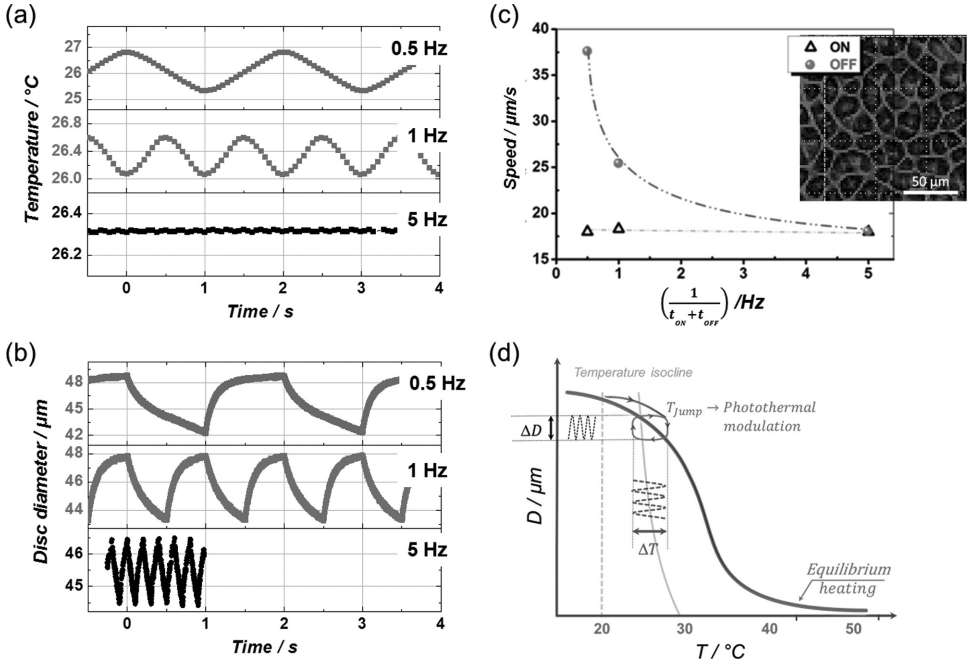

Figure 2. a) Temperature variation in an AuNR solution under modulated irradiation. The modulations have equal on/off durations. Laser intensity: 0.34 W mm^{-2}, optical density of the solution at 808 nm: 76.4 (measured on a cuvette with an optical path: 1 cm), for an irradiated volume of the solution of 1 mm^3, the number density of AuNRs is 2.9 per μm^3. b) Diameter variation of a disk-shaped microgel (as-prepared diameter: 30 μm, thickness: 5 μm) under modulated irradiations. c) Variations of the initial expansion and contraction speeds with the strobe frequency. The inset depicts a confocal image taken in reflection mode of the surface of a substrate-supported hydrogel layer showing a transient instability as it evolves during an intense irradiance. d) Illustration of the diameter variation of a disk under equilibrium heating (thick, dark line) and upon stroboscopic irradiation under nonequilibrium dynamics (cycle shown). A Carnot-like cycle results as the temperature changes faster than the volume.

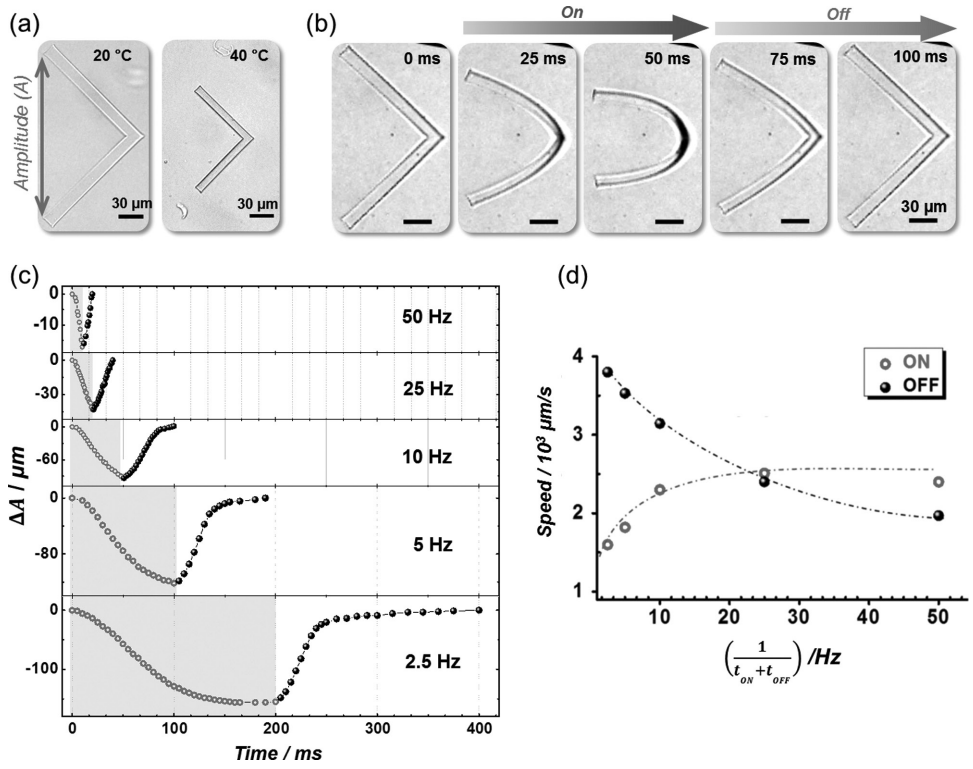

Figure 3. a) Optical microscopy images of the L-shaped microgel in equilibrated state at different temperatures. b–d) Photothermal actuation of an L-shaped hydrogel ribbon (arm length = 100 µm, width 10 µm, thickness 5 µm). b) Characteristic optical images at different stages of the configurational transformation under laser modulation. The modulation has equal on/off periods (50 ms each). c) Variation of the end-to-end amplitude as a function of time during irradiation and recovery. d) Speed of the motion of the ends toward each other and away from each other. Selected movies of the motion appear in the Video S2 and S3 in the Supporting Information.

the inner volume of the microgel object. The wrinkles and thus the denser surface layer only vanished when the gel was practically fully collapsed. The denser surface layer controls the diffusion of water out of the gel and thus its collapse. In contrast, reswelling is promoted by the elastic stress of the swollen outer gel layers. Hence, even for the only 5 µm thick disks we can realize volume variations that do not follow the equilibrium volume/temperature transition but yield a dissipative Carnot-cycle as depicted in Figure 2d.

Morphing rates of 40 µm s^{-1} are already in the range of natural pulsating systems like a beating heart cell or microorganisms like a paramecium.[23] Even faster rates can be realized, if the volume change is exploited to cause bending deformations. This is demonstrated below at the example of an L-shaped microgel object with arms that were much longer than their thickness (**Figure 3**). In order to effectuate bending or buckling the volume change must, however, be locally different within the hydrogel object. Hence, concave bending will be observed, if the upper side of a sheet expands less than its lower side. Heterogeneous volume changes and thus bending can be effectuated, when the swelling or shrinkage is kinetically controlled, i.e., out of equilibrium. This is demonstrated in Figure 3a,b. When the L shaped object was collapsed by slow temperature raise under equilibrium conditions, it shrunk homogeneously without bending (Figure 3a). If, however, the collapse was effectuated by fast temperature changes under nonequilibrium conditions, shrinkage varied throughout the structure depending on the surface to volume ratio in the different sections of the L-shaped body and the L responded by bending the arms together like a tweezers (Figure 3b). Here shrinkage is particularly anisometric for the volume element that connects the two arms (a more detailed analysis is reserved to a special publication). The different states of the L-ribbon in Figure 3b depicts the deformation cycle as observed upon stroboscopic irradiation with periods of 0.05–0.05 s (Video S2, Supporting Information). The time-dependence of the variation of the end-to-end distance, denoted as ΔA, demonstrates a remarkably large distance variation of 156 µm at 2.5 Hz and 122 µm at 5 Hz. The peak velocities were close to 2000 µm s^{-1} at an on/off period of 20 ms and lower at lower frequencies (Figure 3d). Also in this case, the rates of the shape variation depend strongly on the irradiation frequency. While at high frequency, the rate of expansion was slower than the rate by which the ends were moved together, at low frequencies, the expansion was nearly four times faster.

The data from Figure 2 and 3 demonstrate that the course and the rate of the shape change depends on the rate and the depth of the temperature jump but also on formation of diffusion barriers, as the factors which determine the deviation from the equilibrium transition line.

Having understood qualitatively the intriguing motion, that can be achieved by the fast heating and the nonequilibrium

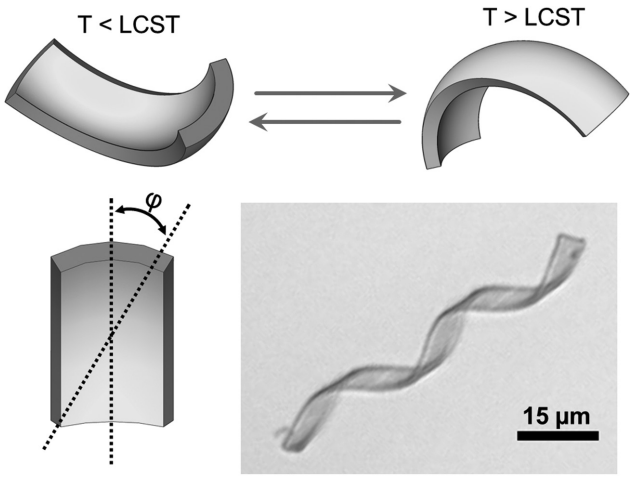

Figure 4. The helix direction is controlled by the principle curvatures $1/R_1$, $1/R_2$ and the mismatch of φ toward the length axis of the ribbon. The optical microscopy image shows the helical microgel at 32 °C.

response and taking advantage of the amplification of the amplitude of motion when a volume change is transformed into bending, we designed a microgel object that can undergo bending also under equilibrium conditions. This should allow an even more rigorous and broader control of the motion. Ribbon or stripes of the GNR equipped hydrogel were coated with a gold skin of a few nanometers in thickness. Different than in the case of the L-shaped ribbon, the coated hydrogel will bend also under equilibrium conditions when the swelling is changed compared to the state when the gold skin was applied (as prepared in the mold). Swelling in cold water causes expansion of the hydrogel layer, while the gold layer is in first instance invariant. The volume collapse of the hydrogel at elevated temperature causes shrinkage of the hydrogel compared to the initial state. In the first case the gold surface is bent in a convex way, in the second case in a concave way. Because bending can occur into the two main directions,[24] i.e., the 80 μm long axis and the 5 μm short axis, an elliptical double curved dome shape is expected as shown in **Figure 4**.

For such a stripe and depending on the width to length ratio and the thickness of the two layers, it is well known, that bending can be preferentially around the long axis of the stripe, resulting in the formation of a tube or around the short axis, resulting in the formation of a 2D spiral. Intermediate situations cause formation of a helix. Whether the helix turns right or left handed depends on small mismatches of the main stress axis and the long axis of the stripe[12] caused by inhomogeneity in the thickness, the bulk structure, or even edge effects.[25] We have controlled whether a spiral or a helix was formed by the thickness of the applied gold skin (Figure S9, Supporting Information). **Figure 5**a depicts optical microscopy images of the helix formed by a hydrogel ribbon with a thickness of 1 μm, a width of 5 μm, and a length of 80 μm that was coated on one (5×80) μm^2 face by a gold layer of 2 nm thickness. In cold water the hydrogel expanded in volume by a factor 5 and the particular ribbon formed a right handed helix with the gold layer facing inside (the rotational direction can be deduced from the Video S5 in the Supporting Information, but is not of importance for the discussion here). In the particular case shown in Figure 5a, the helix length at 20 °C was 72 μm compared to a contour length of 80 μm, and the helix comprised three turns.

When the temperature was raised slowly the hydrogel layer contracted and the helix pitch increased from 5 μm at 20 °C to 31.9 μm at 30.5 °C. The same transformation could be effectuated dynamically when the sample was irradiated by laser light at 808 nm. Because the plasmon resonance of the gold skin is shifted to lower wavelength it contributed at 808 nm only 0.092 to the optical density of the 1 μm thick microgel layer containing 9 GNRs per cubic micrometer, OD = 0.024. Taking into account that the heat conversion efficacy of the gold nanorods is at least an order of magnitude larger than that of thin gold layer,[26] we consider that the heating effects were only slightly enhanced by the gold layer, also gradients in swelling within the 1 μm thick hydrogel layer can be neglected.

Comparison of the optical microscopy images in Figure 5a, i.e., before internal heating by light and 5 ms after switching on the irradiation, demonstrates the response of the helical shape. The change can be characterized quantitatively by the time dependence of the total length and the diameter of the helix. This is shown in Figure 5b for a cycle within a repetitive heating and cooling sequence with an on-time of 16 ms followed by an off-time of 20 ms at 808 nm and 1.7 W mm^{-2}; the external temperature was set to 20 °C. Each on-off cycle comprises two deformation modes, contraction involving volume change, and bending which occurs at a nearly constant volume. Upon heating the helix unwinds, within 15 ms, and at the onset of cooling, it snaps back within 8 ms to its initial radius. The fact, that the shape conversion can be effectuated by raising the temperature of the bath in equilibrium (see Figure 5c) as well as by dynamic heating from inside allows evaluation of the temperature during the irradiation caused temperature changes. The minimum and maximum helix stretching in the stroboscopic irradiation cycle ΔL = 76–72 μm corresponded to a ΔT of less than 10.5 °C (see Figure S11, Supporting Information).

The minimum response time for swelling and unswelling the hydrogel layer by 100 nm in thickness (10 vol%) can be estimated form the diffusion coefficient of water to be less than 1 ms. The slower response times observed in the experiment indicate retardation by the formation of a diffusion controlling skin layer and by the viscous drag on the ribbon. Both effects do cause deviation from the in-equilibrium transition path. The conclusion that the deformations occur off-equilibrium is confirmed by the geometrical description of the cycle in Figure 5d. The figure maps the changes in the diameter relative to length during one power-on and recovery stroke as recorded with a time resolution of 1 ms. During the first 2 ms of irradiation, the helix even contracted in length with a minor change of its diameter. By contrast, during the remaining 14 ms of irradiation, the helix unwound and the diameter increased while the length extended to approach the contour length of the ribbon. Once the light was switched off, again an initial length contraction was followed by twisting of the helix at rather constant length. It can be noted that the sandwich structure of a metal-film on a hydrogel enabled on one side an improved control and predictability of the volume-to-bending deformation and that on the other side, the motion can still be manipulated by nonequilibrium effects even for the rather thin hydrogel film.

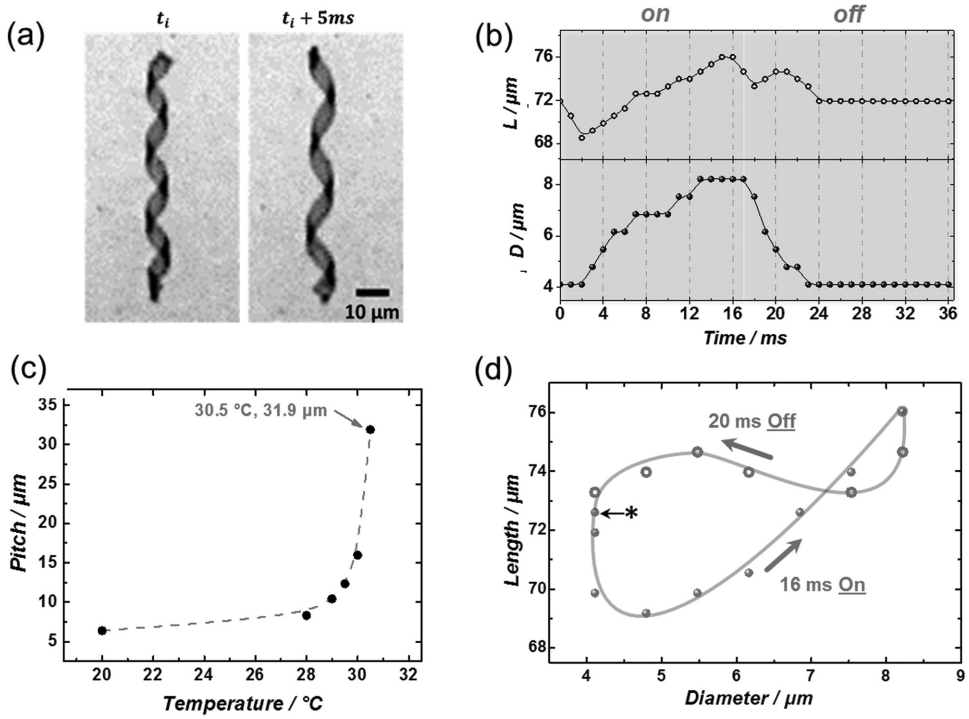

Figure 5. Actuation characteristics of a microgel ribbon helix under stroboscopic irradiation. a) Microscopy images from time-lapse videos of the helix during irradiation. b) Instantaneous helix length and diameter during one irradiation cycle. The left part corresponds to when the light is on, while the right part corresponds to when the light is off. c) The temperature dependent pitch change of the helix in equilibrated state. d) Time evolution of the angular displacement as measured by a time-resolved sequence of time-lapse videos over five cycles. e) The trajectory of the shape deformation in phase space: the helix length versus diameter during a 16 ms power stroke followed by 20 ms recovery period at intervals of less than 2 ms. (*) indicates the starting point at 20 °C.

In summary, Figure 5d shows that not only the time dependencies of the forward and backward motion are different, but also that the geometrical paths are different. Such a nonreciprocal deformation has been cited above as an essential condition for swimming at low Reynolds numbers. Indeed photothermal switching resulted in a quite remarkable double rotation of the helix, which fulfilled the expectation for a directed swimming motion: this is most evident, when the morphing helix is confined in the rectangular capillary for microscopic observation. The confinement within two glass surfaces forces the helical ribbon to stay in the observation plane, but furthermore, the helix presents a freely swimming object. Irradiated by the 16/20 ms on-off sequence, the helix rotates around an axis normal to the long axis and with a much higher rate around its long axis. In **Figure 6**a,

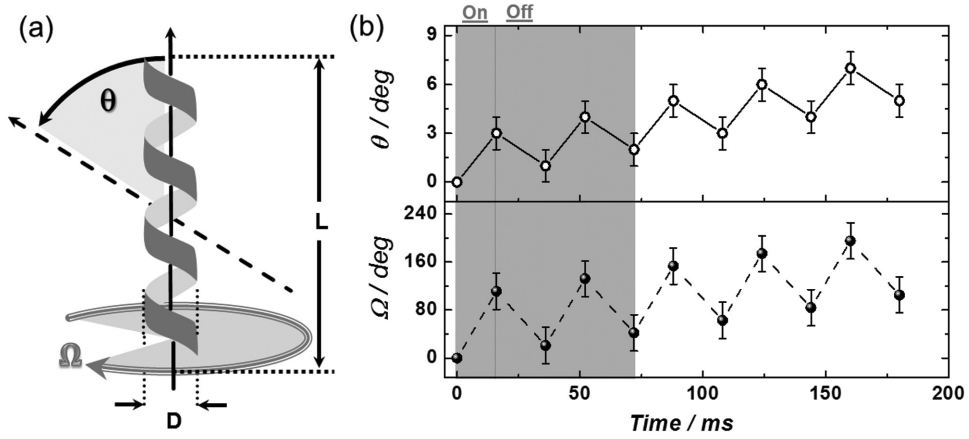

Figure 6. a) Upon periodic irradiation and the associated fast heating and cooling, the gel object revolved simultaneously around two principal axes of the cylindrical helix denoted by the angle Ω on the long axis and θ around normal to the long axis at the center. b) Time evolution of the angular displacement for both rotations as measured by a time-resolved sequence of optical microscopy images. See the Supporting Information for details. Each on/off cycle of irradiation lasts 36 ms, and the laser is on for 16 ms.

the rotation angles have been denoted Ω and θ. Movies of the actuated helix are presented in the Supporting Information; Video S4 in the Supporting Information presents the observed motion in real time. Figure 6b depicts the time dependence of Ω and θ with regard to the on-off steps. The rotation around the normal of the main axis of the helix clearly displayed a sequence of forward and backward steps with a backward step that was smaller than the forward step. The averaged velocity of multiple steps resulted to 31° s^{-1}. For the rotation around the principal axis of the helix, we expect that it is composed of forward and backward steps. Winding of a right handed helix is effectuated by right hand twist. Correspondingly unwinding of a right handed helix requires a left handed twist. So the helix should also rotate around its long axis in an oscillatory way. Although it is difficult to determine the rotational direction in an unambiguous way from the optical microscopy images, this is in agreement with the slow motion Video S5 and the time lapse Video S7 in the Supporting Information that give evidence about a forward and backward turn. Complementarily, the time lapse Video S6 in the Supporting Information that was composed of the respective last frames of 50 subsequent onphases demonstrates continuity of the right handed net rotation. For the net rotation we determined an angular velocity of 590 ± 50° s^{-1} from Video S6 in the Supporting Information. Evidently, the chirality of the helix defines the direction of rotation. Noteworthy here is that the ratio of the mean angular velocities correlates to the diameter of the helix divided by its length, thereby suggesting coupling between the two orthogonal rotations.[27]

If the helix ribbon in water, i.e., at very low Reynolds number, undergoes a net rotation into one direction, it should necessarily translate forward. This is the mechanism of flagellar propulsion observed for many microorganisms. In the case discussed above the thrust is, however, diverted to a rotation around the normal axis. Microorganisms control the directionality by the drag of their body and by employing counterrotating couples of flagella. In an analogous approach we succeeded to navigate the oscillating helix by contact to a flat wall that obstructs the rotation around the axis normal to the helix direction. **Figure 7** and Video S8 in the Supporting Information demonstrate how the rotational motion of the helical ribbon is directed to yield a straight forward motion. The helical ribbon translates along the wall at a velocity of 24.7 µm s^{-1}, a rate that is comparable with that of helical bacteria such as *Spirochaeta*.[28]

In conclusion, we have shown for the purposefully shaped microhydrogels that the kinematics of a cyclic body shape variation can be tuned to differentiate between the forward and the backward motion. Thus, the first deformation stroke (upon heating) is not reciprocated by the second deformation stroke (during cooling), even though the cycle ends up at its starting configuration. Based on this, we have designed a light-fueled and light-controlled microswimmer that can rotate and move forward by its body deformation. Swimming by body shape deformation is distinguished by versatility and control from the motion of a compact body that is self-propelled by thermophoresis,[29] diffusiophoresis,[30] or jetting.[31] Hence, the data shown so far point out further perspectives to design the modes, sequences, and amplitudes of complex

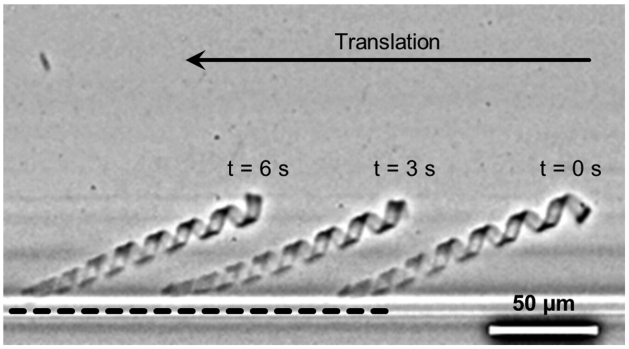

Figure 7. Directing the rotational motion to a linear translocation when the oscillating helix is confined close to a flat wall that impedes the rotation around the axis normal to the helix direction. In this case, the helical ribbon translates along the wall at an on/off frequency of 10/20 ms and a light intensity of 1.7 W mm^{-2}. The speed of the longitudinal movement was 20 µm s^{-1}—a rate comparable to that of slow microorganisms. The helix contour length is 160 µm, the dashed line indicate the wall position.

body deformations of small hydrogel objects precisely and purposeful. Moreover, the locally controlled plasmonic heating exploited in this study for microgel actuation can be easily transferred to liquid crystalline elastomers.[11] Consequently, the self-propulsion of microgels by dynamic control of shapes through photothermal heating provides an exciting avenue for developing soft microrobotics in biomedical or biomechanical applications. In first instance, this approach may be useful for designing new microfluidic devices that can mix, sort, and circulate fluid.

In detail, plasmonic heating of purposefully shaped microhydrogels with embedded gold nanorods enabled a highly differentiated control of shape deformation. Regulation of the length, intensity, and sequence of IR-light pulses, allows controlled motion sequences. As the objects are heated from inside, fast upward but also fast downward temperature jumps are feasible. The latter is possible, because the bath around the microhydrogels is not heated and can dissipate the thermal energy with negligible or imperceptive warming. As a consequence, the volume change can be operated at nonequilibrium conditions, because of the imparity of heat and mass diffusion rates as well as because of heterogeneous shrinking dynamics, As a consequence one can control not only the time response but also the transformation of volume changes to bending and distortion modes. Prestressing to a helical ribbon could be devised by covering a hydrogel microribbon with a thin gold layer. Swelling or unswelling of the hydrogel layer caused formation of a helical configuration. The prestressed state deformed already at small changes in the volume and thus provided a more accurate and sensitive control of the kinematics of the movement. On the one hand, the actual movement of the helical ribbon can be manipulated by adjusting the imbalance of the temperature jump rates and the shrinkage/swelling response rates. On the other hand, the response rate depends also on the path of motion, i.e., the viscous drag is influenced by the orientation of the anisometric microgel relative to the direction of motion. For example, a forward stroke with the ribbon oriented face-on to the motion direction will experience a different viscous drag than a backward stroke, when the ribbon is oriented edge-on relative to the motion.

Supporting Information

Supporting Information is available from the Wiley Online Library or from the author.

Acknowledgements

This work was supported by the German Science Foundation (DFG) within the priority program Microswimmers—from single particle motion to collective behavior (SPP 1726). M.M. acknowledges support by the ERC Advanced Grant 695716.

Note: The institute name in the author affiliation was corrected on January 4, 2017, after initial online publication. The captions of Figure 2 and Figure 5 were also corrected.

Received: September 7, 2016
Revised: September 20, 2016
Published online: November 7, 2016

[1] a) M. Kim, A. A. Julius, E. Steager, *Microbiorobotics: Biologically Inspired Microscale Robotic Systems*, Elsevier, Watham, MA, USA **2012**; b) G. H. Kwon, J. Y. Park, J. Y. Kim, M. L. Frisk, D. J. Beebe, S.-H. Lee, *Small* **2008**, *4*, 2148; c) B. J. Nelson, I. K. Kaliakatsos, J. J. Abbott, *Annu. Rev. Biomed. Eng.* **2010**, *12*, 55; d) M. Sitti, H. Ceylan, W. Hu, J. Giltinan, M. Turan, S. Yim, E. Diller, *Proc. IEEE* **2015**, *103*, 205.
[2] H. C. Berg, *Annu. Rev. Biochem.* **2003**, *72*, 19.
[3] a) F. Vella, *Biochem. Educ.* **1994**, *22*, 164; b) F. Vella, *J. Cell Biol.* **1991**, *114*, 1201.
[4] J. Throndsen, *Nytt Mag. Bot.* **1969**, *16*, 161.
[5] E. M. Purcell, *Am. J. Phys.* **1977**, *45*, 3.
[6] B. U. Felderhof, R. B. Jones, *Physica A: Stat. Mech. Appl.* **1994**, *202*, 94.
[7] If the forward and the backward stroke are identical, the object will return to its starting point.
[8] L. Eric, R. P. Thomas, *Rep. Progress Phys.* **2009**, *72*, 096601.
[9] R. Dreyfus, J. Baudry, M. L. Roper, M. Fermigier, H. A. Stone, J. Bibette, *Nature* **2005**, *437*, 862.
[10] B. J. Williams, S. V. Anand, J. Rajagopalan, M. T. A. Saif, *Nat. Commun.* **2014**, *5*, 1.
[11] S. Palagi, A. G. Mark, S. Y. Reigh, K. Melde, T. Qiu, H. Zeng, C. Parmeggiani, D. Martella, A. Sanchez-Castillo, N. Kapernaum, F. Giesselmann, D. S. Wiersma, E. Lauga, P. Fischer, *Nat. Mater.* **2016**, *15*, 647.
[12] Z. Chen, C. Majidi, D. J. Srolovitz, M. Haataja, *TEX Paper* **2014**, *1209*, 3321.
[13] Z. Chen, C. Majidi, D. J. Srolovitz, M. Haataja, *Appl. Phys. Lett.* **2011**, *98*, 011906.
[14] a) J. M. Skotheim, L. Mahadevan, *Science* **2005**, *308*, 1308; b) P. Fratzl, F. G. Barth, *Nature* **2009**, *462*, 442.
[15] a) P. Kim, L. D. Zarzar, X. He, A. Grinthal, J. Aizenberg, *Curr. Opin. Solid State Mater. Sci.* **2011**, *15*, 236; b) L. Ionov, *Mater. Today* **2014**, *17*, 494.
[16] Y. Hirokawa, T. Tanaka, *J. Chem. Phys.* **1984**, *81*, 6379.
[17] R. Yoshida, T. Takahashi, T. Yamaguchi, H. Ichijo, *J. Am. Chem. Soc.* **1996**, *118*, 5134.
[18] C. M. Pooley, A. C. Balazs, *Phys. Rev. E* **2007**, *76*, 016308.
[19] S. V. Nikolov, P. D. Yeh, A. Alexeev, *ACS Macro Lett.* **2015**, *4*, 84.
[20] T. Tanaka, D. J. Fillmore, *J. Chem. Phys.* **1979**, *70*, 1214.
[21] D. J. Beebe, J. S. Moore, J. M. Bauer, Q. Yu, R. H. Liu, C. Devadoss, B.-H. Jo, *Nature* **2000**, *404*, 588.
[22] J. Xu, D. H. C. Wong, J. D. Byrne, K. Chen, C. Bowerman, J. M. DeSimone, *Angew. Chem., Int. Ed.* **2013**, *52*, 6580.
[23] I. Harary, G. Wallace, G. Bristol, *Cytometry* **1983**, *3*, 367.
[24] E. H. Mansfield, *Proc. R. Soc. London, Ser. A* **1965,** *288*, 396.
[25] a) S. Alben, B. Balakrisnan, E. Smela, *Nano Lett.* **2011**, *11*, 2280; b) J. Bae, J. H. Na, C. D. Santangelo, R. C. Hayward, *Polymer* **2014**, *55*, 5908.
[26] a) J. Dryzek, A. Czapla, *Phys. Rev. Lett.* **1987**, *58*, 721; b) J. Siegel, O. Lyutakov, V. Rybka, Z. Kolská, V. Švorčík, *Nanoscale Res. Lett.* **2011**, *6*, 1.
[27] E. M. Purcell, *Proc. Natl. Acad. Sci.* USA **1997**, *94*, 11307.
[28] a) C. W. Wolgemuth, N. W. Charon, S. F. Goldstein, R. E. Goldstein, *J. Mol. Microbiol. Biotechnol.* **2006**, *11*, 221; b) K. Fosnaugh, E. P. Greenberg, *J. Bacteriol.* **1988**, *170*, 1768.
[29] J. Palacci, C. Cottin-Bizonne, C. Ybert, L. Bocquet, *Phys. Rev. Lett.* **2010**, *105*, 088304.
[30] J. Palacci, S. Sacanna, A. P. Steinberg, D. J. Pine, P. M. Chaikin, *Science* **2013**, *339*, 936.
[31] D. A. Wilson, R. J. M. Nolte, J. C. M. van Hest, *Nat. Chem.* **2012**, *4*, 268.